AEDC-TDR-63-207

# COMPARISON OF DIFFUSER-EJECTOR PERFORMANCE WITH FIVE DIFFERENT DRIVING FLUIDS

By

James W. Hale
Rocket Test Facility
ARO, Inc.

TECHNICAL DOCUMENTARY REPORT NO. AEDC-TDR-63-207

October 1963

AFSC Program Element 62405184/6950

(Prepared under Contract No. AF 40(600)-1000 by ARO, Inc., contract operator of AEDC, Arnold Air Force Station, Tenn.)

ARNOLD ENGINEERING DEVELOPMENT CENTER
AIR FORCE SYSTEMS COMMAND
UNITED STATES AIR FORCE

# NOTICES

Qualified requesters may obtain copies of this report from DDC, Cameron Station, Alexandria, Va. Orders will be expedited if placed through the librarian or other staff member designated to request and receive documents from DDC.

When Government drawings, specifications or other data are used for any purpose other than in connection with a definitely related Government procurement operation, the United States Government thereby incurs no responsibility nor any obligation whatsoever; and the fact that the Government may have formulated, furnished, or in any way supplied the said drawings, specifications, or other data, is not to be regarded by implication or otherwise as in any manner licensing the holder or any other person or corporation, or conveying any rights or permission to manufacture, use, or sell any patented invention that may in any way be related thereto.

# COMPARISON OF DIFFUSER-EJECTOR PERFORMANCE WITH FIVE DIFFERENT DRIVING FLUIDS

By

James W. Hale

Rocket Test Facility

ARO, Inc.

a subsidiary of Sverdrup and Parcel, Inc.

October 1963

ARO Project Nos. RK1319, RM1146, RK0337

AF - AEDC
Arnold AFS Tenn

## ABSTRACT

An investigation was conducted to determine the diffuser-ejector performance for five different driving fluids--air, nitrogen, argon, helium, and hydrogen--having different ratios of specific heats. Two diffuser-ejector configurations, which consisted of two different area ratio nozzles and two duct sizes which gave duct-to-nozzle area ratios of 73.06 and 20.40, were used in this investigation. The nozzle for configuration 1 was an 18-deg, half-angle conical nozzle with an area ratio of 18.00, and the nozzle for configuration 2 was a 7.58-deg, half-angle conical nozzle with an area ratio of 10.76. The stagnation conditions for the driving fluids ranged in pressure from 51 to 866 psia and temperature from 450 to 516°R.

The cell-to-driving fluid pressure ratios ($P_c/P_t$) for the different driving fluids were dependent on the ratio of specific heats, $\gamma$. An increase in $\gamma$ resulting from a decrease in temperature, such as for hydrogen, produced a decrease in $P_c/P_t$. A decrease in $\gamma$ resulting from the change from a single-phase to a two-phase fluid (condensation), such as for air, nitrogen, and argon, caused the $P_c/P_t$ ratios to increase.


## PUBLICATION REVIEW

**This report has been reviewed and publication is approved.**

Eules L. Hively
Acting Chief, Propulsion Division
DCS/Research

Donald R. Eastman, Jr.
DCS/Research

## CONTENTS



## TABLES



## ILLUSTRATIONS

## NOMENCLATURE

| | |
|---|---|
| $A^*$ | Cross-sectional area of nozzle throat, $in.^2$ |
| $A_d$ | Cross-sectional area of diffuser, $in.^2$ |
| $A_{ne}$ | Cross-sectional area of nozzle exit, $in.^2$ |
| $C_p$ | Specific heat at constant pressure, $\frac{Btu}{lb_m - °F}$ |
| D | Diameter of diffuser duct, in. |
| $g_c$ | Standard acceleration of gravity, $32.17 \frac{ft - lb_m}{lb_f - sec^2}$ |
| L | Length of diffuser duct at diameter, D, in. |
| M | Mach number |
| P | Fluid static pressure, psia |
| $P_c$ | Test cell pressure, psia |
| $P_{ex}$ | Diffuser duct exit pressure, psia |
| $P_t$ | Nozzle driving fluid total or stagnation pressure, psia |
| $\left(\frac{P}{P_t}\frac{\dot{m}}{}\right)_{M=1}$ | Mass flow parameter at Mach number of unity, $\frac{lb_m - °R^{1/2}}{lb_f - sec}$ |
| R | Specific gas constant, $\frac{ft - lb_f}{lb_m - °R}$ |
| $Re/\ell$ | Reynolds number per unit length, $ft^{-1}$ |
| T | Fluid static temperature, °R |
| $T_t$ | Nozzle driving fluid or stagnation temperature, °R |
| W | Mass flow rate, $lb_m/sec$ |
| $\gamma$ | Ratio of specific heats |
| $\theta_n$ | Nozzle divergent half angle, deg |
| $\mu$ | Dynamic viscosity, $\frac{lb_m}{ft - sec}$ |
| $\rho$ | Fluid density, $lb_m/ft^3$ |

### SUBSCRIPTS

| | |
|---|---|
| act | Actual |
| isen | Isentropic |

## 1.0 INTRODUCTION

Some fluids have invariant ratios of specific heats with temperature over a wide temperature range, whereas other fluids have a very large variation in the ratio of specific heats with temperature. For most real gases, this variation of the ratio of specific heats with temperature is well defined.

An investigation was conducted to determine if there is a difference in diffuser-ejector performance when using different driving fluids having the same average ratio of specific heats, and if the performance of the diffuser-ejector for one particular driving gas can be used to accurately predict the diffuser-ejector performance for another driving gas, both with the same average ratio of specific heats and with a different average ratio of specific heats.

The five different gases used as the diffuser-ejector driving fluids were air, nitrogen, hydrogen, argon, and helium. Two diffuser-ejector configurations consisting of different nozzles and different diameter diffusers were used in this investigation. Correlation between the data obtained and one-dimensional isentropic relationship as given in Ref. 1 for diffuser-to-nozzle throat area ratio, cell-to-nozzle total pressure ratio, and ratio of specific heats, is shown.

This study was conducted in the Rocket Test Facility (RTF), Arnold Engineering Development Center (AEDC), Air Force Systems Command (AFSC), from October 25 to December 20, 1962.

## 2.0 APPARATUS

The test installation consisted of two diffuser-ejector configurations (Figs. 1 and 2). Each has a single axisymmetric nozzle concentrically located in the diffuser.

### 2.1 DIFFUSER-EJECTOR CONFIGURATION 1

For configuration 1 (Fig. 1), a 4-in. schedule 160 pipe 18 in. long welded to a 6-in. flange was used as the nozzle plenum chamber. The nozzle was installed on the plenum chamber with a gasket and secured

---

Manuscript received August 1963.

by means of eight 1/4-in. bolts. The axisymmetric, 18-deg, half-angle conical nozzle used in configuration 1 (see Fig. 3) had an exit-to-throat area ratio, $A_{ne}/A^*$, of 18.00 with a throat diameter of 0.471 in. The plenum section was located in a sealed test cell section to which the diffuser was attached (see Fig. 1).

The test cell in which the nozzle plenum section was installed consisted of a duct 12 in. in diameter and 20 in. long. A 24-in.-long duct 4.026 in. in diameter called the diffuser was connected to the downstream face of the test cell and the upstream face of the 20-in.-diam exhaust ducting.

## 2.2 DIFFUSER-EJECTOR CONFIGURATION 2

For configuration 2 (Fig. 2), the nozzle plenum section consisted of a 1-in. schedule 80 pipe 2.5 in. long; one end of which was welded to a 4-in. flange and the other end internally threaded for installation of the nozzle with an "O"-ring seal. The axisymmetric, 7.58-deg, half-angle conical nozzle used in this configuration and shown in Fig. 4 had an exit-to-throat area ratio, $A_{ne}/A^*$, of 10.76 with a throat diameter of 0.304 in. The plenum section was located in a sealed test cell section which was a part of the diffuser.

A 3-in. coupling 2 in. long was welded concentrically with the nozzle plenum section to the 4-in. flange. Bushings were used to adapt the 1.373-in. diffuser to the coupling. The diffuser extended 10.94 in. downstream of the nozzle exit. The nozzle and diffuser assembly was installed in a 4-in. duct connected to the exhaust ducting, and the assembly was tested in a remote area with the diffuser discharging to atmospheric pressure.

## 2.3 NOZZLE DRIVING FLUIDS

Air, argon, helium, hydrogen, and nitrogen were used as the nozzle driving fluids for configuration 2, whereas air, argon, and nitrogen were used as nozzle driving fluids for configuration 1. The VKF 4000-psi storage tank supplied the dry air, while the argon, helium, nitrogen, and hydrogen were supplied by K-bottles. From 3 to 20 K-bottles of the particular gas were manifolded together and regulated by a pressure regulating valve to give the desired nozzle driving pressure and sufficient run time for recording the data. The nozzle plenum total pressure was supplied as high as 866 psia. The diffuser-ejector either exhausted to the RTF facility exhaust machines, which maintained exhaust pressure as low as 0.10 psia, or exhausted to atmospheric

pressure (14.22 psia). For both configurations, hand-operated gate valves (Figs. 1 and 2) were used to vary the exhaust pressure at the exit of the diffuser-ejector when the diffuser exhausted to the RTF facility exhaust machines.

### 2.4 INSTRUMENTATION

The parameters of primary interest were cell pressure, exhaust pressure, nozzle plenum total pressure, and nozzle plenum total temperature.

All pressures were read on diaphragm-activated dial gages. The temperature was measured with copper-constantan thermocouple and read on a compensating millivolt meter. All parameters were recorded manually after a steady-state condition was reached. The gages were periodically calibrated, and the readings were well within the calibration range.

## 3.0 TEST PROCEDURE

At the beginning of each test with the exception of the remote area runs, a vacuum check was made to detect any possible leaks into the system before any data were taken.

The objective of the test was to determine the performance of each configuration as a diffuser-ejector by finding the minimum cell-to-nozzle total pressure ratio and the corresponding starting and operating pressure ratios for each of the nozzle driving gases.

The pressure ratio, $P_c/P_t$, was determined both for air and nitrogen by varying the nozzle inlet total pressure. From these data, the minimum nozzle inlet total pressure at which $P_c/P_t$ remained constant was determined (Reynolds number influence as given in Ref. 2). The minimum nozzle inlet total pressure for hydrogen, argon, and helium was calculated from the pressures determined for air and nitrogen. These pressures were calculated from the equal Reynolds number per unit length relationship based on nozzle throat flow conditions (derived in Appendix I):

$$\frac{Re}{\ell} = \frac{\left[\frac{P}{P_t}\dot{m}\right]_{M=1} P_t}{\sqrt{T_t}\ \mu^*} = K\ P_t$$

where K is a constant for a particular gas.

## 4.0 RESULTS AND DISCUSSION

The primary purpose of this experimental investigation was to determine if, by knowing the ratio of specific heats of a particular driving gas, the performance of a diffuser-ejector could be predicted from the one-dimensional isentropic relationship as given in Ref. 1. Only two diffuser-ejector configurations were used in the test. The important parameters of the configurations are:

| Configuration | Diffuser Diam, D, in. | Ratios | | | $\theta_n$ |
|---|---|---|---|---|---|
| | | L/D | $A_{ne}/A^*$ | $A_d/A^*$ | |
| 1 | 4.026 | 5.71 | 18.00 | 73.06 | 18° |
| 2 | 1.373 | 7.97 | 10.76 | 20.40 | 7.58° |

### 4.1 PROPERTIES OF THE SELECTED DRIVING FLUIDS

The average thermodynamic properties (R, $\gamma$, $C_p$, and $\mu$) at 1-atm pressure and ambient temperature for the five driving fluids used were taken from Refs. 3, 4, and 5 and are presented in Table 1. It was desirable to have a constant property gas (a gas with properties not variant with temperature and pressure, especially the ratio of specific heats). Taken from Refs. 4 and 5 and presented in Fig. 5 are the effects of pressure and temperature on the ratio of specific heats, $\gamma$, for the driving gases air, argon, helium, hydrogen, and nitrogen. Air, nitrogen, and argon at 0.1-atm pressure and helium at 1-atm pressure have ratios of specific heats which are practically independent of temperature even down to very low temperatures (between 100 and 200°R), but $\gamma$ does vary with temperature for air and nitrogen at temperatures above 600°R.

For hydrogen gas at temperatures below 600°R, the variation of $\gamma$ with temperature is quite large: from 1.40 at 600°R to 1.66 at 120°R for 1-atm pressure. Only a slight change in the temperature-ratio of specific heats relationship was noticeable in the low-temperature range when the pressure was reduced to zero. As much as 40-atm pressure alters the relationship of temperature and $\gamma$ for hydrogen or the other gases but little (see Refs. 4 and 5). The hydrogen curve in Fig. 5 indicates that for stagnation temperatures around 600°R hydrogen does not behave as a constant property fluid when expanded through a convergent-divergent nozzle. The ratio of specific heats for hydrogen is a strong function of temperature.

The static temperature of a constant property fluid drops as the area increases downstream of the nozzle throat in the divergent portion of a nozzle according to the isentropic relationships given in Ref. 6, which are

$$A/A^* = \frac{1}{M}\left[\left(\frac{2}{\gamma+1}\right)\left(1 + \frac{\gamma-1}{2} M^2\right)\right]^{\frac{\gamma+1}{2(\gamma-1)}} \quad \text{and}$$

$T_t/T = 1 + \frac{\gamma-1}{2} M^2$ and are tabulated in Ref. 1. When $\gamma$ is dependent on the local static temperature as in hydrogen gas expansion for stagnation temperature around 600°R, the above equations are still valid, but $\gamma$ becomes a variable.

Presented in Fig. 6 are the $T/T_t$ vs $A/A^*$ isentropic expansions for gases with constant and variable ratios of specific heats (for thermal equilibrium flow). The $\gamma = 1.40$ curve represents air and nitrogen, and the $\gamma = 1.67$ curve represents helium and argon. Actually there is a small difference in $\gamma$ for helium and argon as presented in Fig. 5. The dashed curve which starts approximately at the $\gamma = 1.40$ isentrope increases with decreasing temperature ratio, $T/T_t$, for an increasing area ratio, $A/A^*$, to the $\gamma = 1.67$ isentrope and represents the isentropic thermal equilibrium expansion of hydrogen for a stagnation temperature of 500°R. The dashed vertical lines represent the nozzle area ratio, $A_{ne}/A^* = 10.76$, and duct-to-nozzle throat area ratio, $A_d/A^* = 20.40$.

### 4.2 START AND BREAKDOWN PRESSURE RATIO PERFORMANCE

Table 2 is a summary of all the data obtained for the two configurations with the various driving gases. The respective isentropic values and the actual data deviation from isentropic values are shown. Presented in Fig. 7 for the two diffuser-ejector configurations are the start and breakdown pressure ratios for the different driving gases in relation to their respective theoretical one-dimensional, normal shock, total pressure ratios ($P_{ty}/P_{tx}$ where x is upstream of normal shock and y is downstream).

For the small configuration (configuration 2) all five gases--air, argon, helium, hydrogen, and nitrogen--were used as driving fluids. Air and nitrogen, which have almost the same ratio of specific heats (Fig. 5) differed in $P_{ex}/P_t$ at breakdown by approximately 10 percent. The breakdown pressure ratio for nitrogen was 0.0677 which was 90.22 percent of the theoretical one-dimensional normal shock value. This 90.22 percent of normal shock total pressure ratio value for the

L/D = 7.97 for the diffuser configuration 2 is in good agreement with that presented in Fig. 6 of Ref. 7 and Fig. 10 of Ref. 8 for air as the driving fluid. The $P_{ex}/P_t$ for air in this investigation was 81.21 percent of the normal shock total pressure ratio. This difference in $P_{ex}/P_t$ obtained for air and nitrogen driving gas may be a result of the difference in the method of determining the breakdown pressure ratios for the two gases. The $P_{ex}/P_t$ ratio for air was determined for a set driving pressure $P_t$, and the exhaust pressure was varied (see Fig. 2a) until the cell pressure started to increase. The nitrogen $P_{ex}/P_t$ ratio at breakdown was determined by discharging the diffuser to atmospheric pressure (Fig. 2b) and decreasing the driving pressure until the cell pressure started to increase.

For configuration 1 (Fig. 1, large area ratio, $A_d/A^* = 73.06$), the breakdown pressure ratio for air and nitrogen were determined in the same manner as for air in configuration 2. Air gave a breakdown pressure ratio of 77.52 percent of the normal shock total pressure ratio, $P_{ty}/P_{tx}$, whereas nitrogen gave a ratio of 80.52 percent of the normal shock value. The L/D for the configuration 1 diffuser was 5.71. When compared with the results shown in Refs. 7 and 8, this L/D ratio of 5.71 for the breakdown pressure ratios of 77.52 and 80.52 percent of normal shock $P_{ty}/P_{tx}$ shows good agreement. This comparison and that presented above for configuration 2 indicate that the $P_{ex}/P_t$ ratio for configuration 2 with air driving fluid is low.

Only three (air, nitrogen, and argon) of the five gases were used for driving fluids in configuration 1. The breakdown pressure ratio, $P_{ex}/P_t$, for argon was 73.58 percent of the theoretical, one-dimensional, normal shock, $\gamma = 1.67$, total pressure ratio. This 73.58 percent of normal shock value was lower than the value obtained for air (77.52 percent), but all three ratios $\left[(P_{ex}/P_t)_{act}/(P_{ty}/P_{tx})\right]$ were within a 9-percent spread.

The remaining driving gases used in configuration 2 (argon, helium, and hydrogen) gave $P_{ex}/P_t$ ratios in percent of normal shock total pressure ratio as 94.25 percent for argon, 83.43 percent for helium, and 97.26 percent for hydrogen. The ratio for hydrogen was computed, based on a $\gamma = 1.67$ as shown in Fig. 6, at the nozzle exit. Actually the static temperature rises as the stream shocks down and approaches the diffuser exit. This rise in static temperature causes a decrease in $\gamma$ toward 1.40 for hydrogen. The normal shock total pressure ratio for a $\gamma = 1.40$ is higher than for a $\gamma = 1.67$; therefore, for a $\gamma = 1.40$ the $P_{ex}/P_t$ in percent of normal shock $P_{ty}/P_{tx}$ is 88.54 percent. This value is in line with nitrogen (90.22 percent) and is believed to be the more reliable value. The difference in the breakdown pressure ratios

in percent of the normal shock total pressure ratios for the various driving gases for a particular configuration are considered to be data scatter and the results of $\gamma$ variation with pressure and temperature. An insufficient number of breakdown points was obtained for determining a mean value of $\left[(P_{ex}/P_t)_{act}/(P_{ty}/P_{tx})\right]$ for each driving gas.

### 4.3 CELL PRESSURE RATIO VARIATION WITH NOZZLE PLENUM TOTAL PRESSURE

Presented in Fig. 8 for the different driving gases is the performance variation of the cell pressure ratio, $P_c/P_t$, for various nozzle driving total pressures. Air and nitrogen were used for locating the optimum driving pressure (driving pressure at which the lowest cell pressure ratio occurred as presented in Ref. 2) from which driving pressures for argon, helium, and hydrogen were determined. The driving pressures for the various driving fluids were related such that the nozzle throat Reynolds number per unit length for the different gases would be equal. The Reynolds number per unit length equation as derived in Appendix I is

$$\frac{Re}{\ell} = \frac{W}{A^* \mu^*} = \frac{\left[\frac{P}{P_t}\dot{m}\right]_{M=1} P_t}{\sqrt{T_t}\ \mu^*} = K\ P_t$$

where K is a constant for a particular gas. For equal nozzle throat Reynold number per unit length, the equation becomes

$$K_A\ (P_t)_A = K_B\ (P_t)_B = K_C\ (P_t)_C$$

where subscripts A, B, and C represent different gases.

Based on the optimum driving pressure of approximately 300 psia, as presented in Fig. 8 for air and nitrogen, the desired driving pressures for argon, helium, and hydrogen from the above equation are 300 psia for argon, 859 psia for helium, and 568 psia for hydrogen based on a nozzle stagnation temperature of 470°R for each gas. It is not known if these driving pressures are optimum for helium and hydrogen because in Fig. 8 the cell pressure ratio was still decreasing at the 866-psia pressure level. No pressure higher than 866 psia was investigated for helium. Only one pressure level was investigated for hydrogen (651 psia).

The air and nitrogen cell pressure ratio variations with nozzle stagnation pressure are practically the same curve. This was expected since the major portion of air is nitrogen.

## 4.4 MINIMUM CELL-TO-NOZZLE STAGNATION PRESSURE RATIO DEVIATION FROM ISENTROPIC

Since air and nitrogen have almost the same ratio of specific heats and are almost invariant with temperature below 600°R (see Fig. 5), the same minimum cell-to-nozzle stagnation pressure ratios were expected for a given diffuser-ejector and equal stagnation pressures and temperatures. For the same reasons, argon and helium should give the same minimum cell-to-nozzle stagnation pressure ratio. There is only a slight difference in their ratios of specific heats as presented in Fig. 5.

Presented in Fig. 9 are the minimum cell-to-nozzle stagnation pressure ratios obtained for the various driving gases in the two diffuser-ejector configurations in relation to their respective isentropic ratios. The air and nitrogen $P_c/P_t$ ratios were equal for each respective configuration. The ratios $P_c/P_t$ for air and nitrogen for configuration 1 are slightly above the $\gamma = 1.40$ isentrope $[(P_c/P_t)_{act}/(P_c/P_t)_{isen} = 1.183$ for air and 1.123 for nitrogen$]$. For configuration 2, the $P_c/P_t$ ratios for air and nitrogen are below the $\gamma = 1.40$ isentrope $[(P_c/P_t)_{act}/(P_c/P_t)_{isen} = 0.426$ for air and 0.429 for nitrogen$]$. A difference in $(P_c/P_t)_{act}/(P_c/P_t)_{isen}$ for the two configurations was expected because they differed in (1) nozzle half angle, (2) nozzle area ratio, and (3) duct-to-nozzle throat area ratio.

An increase in the ratio of the actual $P_c/P_t$ to the isentropic pressure ratio with increasing duct-to-nozzle throat area ratio is shown in Refs. 7 and 8. A decrease in nozzle half angle resulting in a decrease in the actual-to-isentropic pressure ratios is presented in Ref. 7 and has been noted in preliminary investigations. From other preliminary work, a decrease in nozzle area ratio from 18.00 to 5.0 resulted in an increase in $P_c/P_t$ from 1.51 to 3.19 times the corresponding isentropic pressure ratios. The three geometric differences in the two configurations were expected to result in similar performance differences regardless of the driving gas used. The $P_c/P_t$ performance effect from a $\gamma$ change as a result of fluid condensation will be discussed later.

When argon was used as the driving fluid for the two configurations, the ratios of the actual $P_c/P_t$ to the isentropic pressure ratio $[(P_c/P_t)_{act}/(P_c/P_t)_{isen}]$ were 5.931 for configuration 1 and 1.579 for configuration 2. Both configurations had $P_c/P_t$ ratios greater than the isentropic ratio. The other driving gas (helium, $\gamma = 1.66$) used only in configuration 2 had practically the same ratio of specific heats as argon ($\gamma = 1.67$ in Fig. 5). The ratios $(P_c/P_t)_{act}/P_c/P_t)_{isen}$ obtained with

helium driving gas were 0.647 for a driving pressure of 575 psia and 0.575 for a driving pressure of 866 psia. From section 4.3, the driving pressure of 866 psia should give the minimum $P_c/P_t$ ratio. The difference in the diffuser-ejector performance in $P_c/P_t$ with argon and helium driving gases in configuration 2 will be discussed in sections 4.5 and 4.6 as a driving fluid condensation effect.

Hydrogen (the variable ratio of specific heats gas below 600°R) was used as the driving fluid in configuration 2. As shown in Fig. 5 and the expansion in Fig. 6, $\gamma$ varies from approximately 1.41 at 500°R to approximately 1.67 at 100°R with little variation as a result of the pressure change. Since near the end of the nozzle ($A_{ne}/A^* = 10.76$), $\gamma$ approaches 1.67 for hydrogen (see Fig. 6), the isentropic ratio of cell-to-stagnation pressure was based on $\gamma = 1.67$. The actual $P_c/P_t$ ratio obtained for hydrogen as presented in Fig. 9 was the same value as that obtained for helium. The ratio $[(P_c/P_t)_{act}/(P_c/P_t)_{isen}]$ for hydrogen was 0.648 for a driving pressure of 651 psia. This 0.648 value is the same as that obtained for helium at a driving pressure of 575 psia. The fact that helium and hydrogen driving gases pumped the same minimum $P_c/P_t$ in configuration 2 indicates that the two gases had the same effective $\gamma$. Since only one size diffuser was used in this investigation ($A_d/A^* = 20.40$) for hydrogen and helium driving gas, it is not known whether the $P_c/P_t$ would still depend on the nozzle exit $\gamma$ for larger diffusers where the expansion from the nozzle exit would drop the driving gas static temperature even more. In Fig. 5, the zero-atm pressure line for hydrogen indicates that as temperature continues to drop from 100°R toward zero, $\gamma$ does not exceed a value of approximately 1.67. From this fact, it can be concluded that $P_c/P_t$ is dependent on the constant $\gamma = 1.67$ and $A_d/A^*$. The hydrogen driving fluid condensation effect is also discussed in sections 4.5 and 4.6.

### 4.5 EXPANSION BEYOND THE SATURATION LIMIT

A definite pressure-temperature relationship exists for a fluid in a thermal equilibrium condition between phases such as gas, liquid, and solid. The relationship of pressure and temperature between the gaseous and liquid or solid phases is known as the saturation curve or phase boundary (the condition at which different phases of a fluid will exist in thermal equilibrium). Figures 10 and 11 present the phase boundary (saturation curve) taken from Refs. 4, 5, and 9 for the various fluids used in this investigation. The triple point is shown on the phase boundary curves (Figs. 10 and 11) for the fluids except air and helium. (A state of a fluid at which the liquid, gaseous, and solid phase can exist in thermal equilibrium is referred to as the

triple point.) The superheated state (single gaseous phase) of a fluid exists on the right of the phase boundary curve, whereas a two-phase state (gaseous-liquid or gaseous-solid) exists on the left. This phase boundary curve can be thought of as a thermal equilibrium saturated expansion. The theoretical expansion of a fluid through a convergent-divergent nozzle gives a different curve known as an isentropic thermal equilibrium expansion (a reversible process with no heat transferred across the boundary or a constant entropy process). This isentropic expansion curve is presented in Figs. 10 and 11 for the two nozzles used in this investigation. The isentropic expansions presented in Fig. 10 were for a fluid having an invariant ratio of specific heats ($\gamma$ = 1.40) and a variable ratio of specific heats ($\gamma$ = 1.40 to 1.67) with temperature, and stagnation condition of $P_t$ = 300 psia and $T_t$ = 490°R.

The end of the $A_{ne}/A^*$ = 10.76 nozzle shown on the $\gamma$ = 1.40 isentropic expansion curve was on the right (gaseous phase) of the nitrogen phase boundary curve, whereas the $A_{ne}/A^*$ = 18.00 nozzle extended to the left (gaseous-solid phase). As seen in Fig. 5, both air and nitrogen have essentially the invariant $\gamma$ = 1.40 with temperature property. If thermal equilibrium could be maintained throughout the isentropic expansion of air or nitrogen from the stagnation pressure of 300 psia and temperature of 490°R through the $A_{ne}/A^*$ = 18.00 nozzle, an increasing solid-phase, two-phase, gaseous-solid fluid would extend from the point where the isentropic expansion curve crosses the phase boundary curve as shown in Fig. 10. If hydrogen could be considered a constant $\gamma$ = 1.40 fluid, then for the stagnation condition given above and in Fig. 10 the fluid would remain in the single gaseous phase (superheated gas) throughout either nozzle ($A_{ne}/A^*$ = 10.76 or 18.00). For a stagnation temperature no greater than 490°R, Fig. 5 shows that hydrogen is not a constant $\gamma$ gas in an isentropic expansion down to a temperature of approximately 95°R. The $\gamma$ ratio increases from approximately 1.40 to 1.67. Helium and argon have essentially an invariant $\gamma$ of approximately 1.67 with temperature as shown in Fig. 5. A constant $\gamma$ = 1.67 isentropic expansion for stagnation pressure of 228 psia and temperature of 452°R is presented in Fig. 11 with the helium, hydrogen, and argon phase boundary curves (saturation curve). This isentropic expansion for both nozzles ($A_{ne}/A^*$ = 10.76 and 18.00) extends far into thermal equilibrium, two-phase, gaseous-solid, argon fluid region. The helium driving fluid in the above isentropic expansion for the $A_{ne}/A^*$ = 18.00 nozzle never reaches saturation. The fluid is in the single gaseous phase (superheated gas) throughout the expansion.

If hydrogen is considered a constant $\gamma$ = 1.67 fluid and isentropically expanded from the $P_t$ = 228 psia and $T_t$ = 452°R stagnation condition,

again the fluid expansion never reaches the hydrogen phase boundary curve. The hydrogen would remain in the single gaseous phase throughout the nozzle ($A_{ne}/A^* = 18.00$) as shown in Fig. 11. If the stagnation pressure was increased from the $P_t = 228$ while the stagnation temperature remained constant at $T_t = 452°R$, the isentropic expansion curve would move upward. This increase in stagnation pressure would permit the isentropic expansion curve to cross the argon phase boundary curve allowing the argon fluid theoretically to undergo a phase change closer to the nozzle throat (Fig. 11). If $P_t$ were increased to a sufficiently high value with $T_t$ held constant, the hydrogen isentropic expansion curve would approach and eventually cross the hydrogen phase boundary curve.

If the stagnation temperature is increased from the $T_t = 452°R$ value while $P_t$ remains constant at 228 psia, the isentropic expansion curves shift to the right delaying the onset of condensation for argon and allowing hydrogen and helium to be in a higher superheated state when leaving the nozzle (Fig. 11). A higher hydrogen stagnation temperature from Fig. 5 decreases the average $\gamma$, or the $\gamma$ at the end of the nozzle, toward 1.40. This reduction in $\gamma$ would allow the isentropic expansion curve to move still farther to the right of the hydrogen phase boundary curve as shown in Fig. 10.

Air, nitrogen, and argon as driving fluids for the $A_{ne}/A^* = 10.76$ and 18.00 nozzles for stagnation conditions of $P_t$ approximately 300 psia and $T_t$ approximately 500°R undergo a phase change (from a single gaseous phase to two phase) during the isentropic expansion. The fluid-phase-change position in the nozzle can be shifted downstream by either lowering $P_t$ or increasing $T_t$ from the above values. Helium has such a low saturation temperature (Figs. 10 and 11) that an isentropic expansion for the above stagnation conditions with the above nozzles remains in a single phase fluid throughout the expansion. The stagnation temperature would have to be decreased below the 452°R level so that the static temperature at the nozzle exit would be approximately 30°R lower at a constant $P_t = 228$ psia for condensation to theoretically start at the end of the $A_{ne}/A^* = 18.00$ nozzle.

The slope of a variable $\gamma$ ($\gamma = 1.40$ to 1.67) isentropic expansion curve for a specific stagnation condition is different from a constant $\gamma$ isentropic expansion as shown in Figs. 10 and 11. Such an isentropic expansion curve results for hydrogen driving fluid at the stagnation conditions investigated.

## 4.6 DELAYED CONDENSATION IN A RAPID EXPANSION

Flow with condensation has long been a subject of primary interest. J. L. French of RTF has made a study of literature concerning flow with condensation. When an isentropic expansion of a fluid through a nozzle results in the fluid properties leaving a single-phase (superheated gas) and entering a two-phase (gaseous-liquid or gaseous-solid) thermal equilibrium region (see section 4.5), a strange phenomenon occurs. This phenomenon is known as "condensation" (phase change) as reported in Refs. 6, 10, 11, 12, and others for condensable fluids such as steam. It has been observed (Refs. 6 and 12) that in a rapid expansion of steam through a convergent-divergent nozzle condensation is delayed to some point below the thermal equilibrium saturation line. This delay in condensation results in a metastable state known as a supersaturated state (Ref. 11). The supersaturation limit for steam is referred to as the Wilson Line, which lies approximately 60 $Btu/lb_m$ below the line of saturation. Air saturated with water vapor will expand isentropically to a volume 25 percent greater before condensation occurs (Ref. 12). Shown below are a sketch of a nozzle and pressure distribution through the nozzle with condensation and a temperature versus entropy diagram showing an isentropic expansion from superheated state through thermal equilibrium saturation limit to a metastable state.

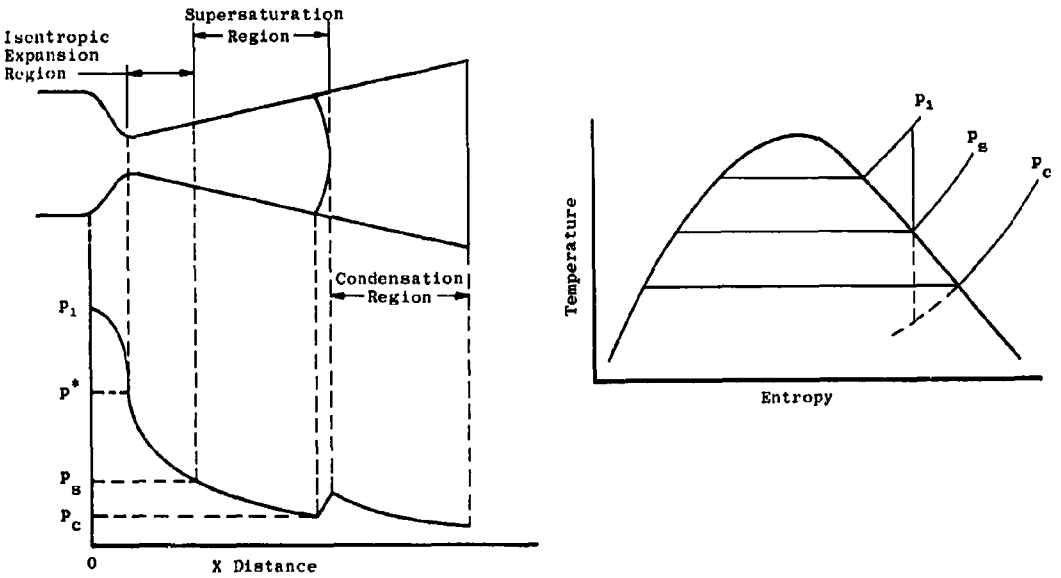


**Typical Characteristic for Steam**

As shown in the nozzle sketch, condensation does not occur when the fluid properties reach the saturation condition in the isentropic expansion but continues to expand apparently isentropically until the supersaturation limit is reached. At the supersaturation limit, a discontinuity in pressure similar to that of a normal shock occurs. This discontinuity is known as a condensation shock. The fluid from the condensation shock through the remaining portion of the nozzle is two phase.

Gases such as the ones used in this investigation have supersaturation limits similar to the Wilson Line for steam. Such supersaturation limits for air, nitrogen, and helium are presented in Refs. 13 through 24. References 15, 17, and 20 show that the supersaturation of nitrogen can be decreased by the addition of impurities such as $CO_2$, water vapor, argon, and oxygen. A fraction of a percent of $CO_2$ or water vapor will eliminate completely all supersaturation. Unlike steam, air (Refs. 14, 16, 19, 21, 22, and 23) and nitrogen (Refs. 13, 15, 16, 21, and 24) do not have the condensation shock when condensation begins as shown in the preceding sketch. A gradual rather than an instantaneous pressure increase due to condensation was evident. Reference 14 indicates that a maximum of 55°F of supersaturation may be obtained for air.

The static pressure rise after the onset of condensation is due to the heat released by the condensing fluid (Ref. 16). This static pressure can be predicted by the saturation expansion theory presented in Ref. 18. The theory is based on the assumption that the expansion through the nozzle follows the isentrope in the pressure-temperature plane until the fluid saturation curve is intersected. Further expansion then follows along the fluid saturation curve. Since there is a static pressure rise after the onset of condensation, it is desirable to have the condensation limit delayed, such as when the fluid expands to a high degree of supersaturation. This supersaturation phenomenon (condensation delay) will allow a lower stagnation temperature fluid to expand apparently isentropically and condensation-free than could be expanded isentropically and condensation-free if supersaturation did not exist. A limiting static pressure range (about 0.077 psia) above which air supersaturation will not occur is reported in Ref. 14.

The Mach number is lower and static pressure is higher at the exit of a nozzle for a condensing fluid (two phase) than it is for a non-condensing fluid (single phase). This lower nozzle exit Mach number and higher nozzle exit static pressure is an effective smaller than actual $A_{ne}/A^*$ nozzle. Only this smaller than actual $A_{ne}/A^*$ nozzle with a given $A_d/A^*$ and a single-phase gaseous fluid will produce a higher test cell pressure.

Since a diffuser-ejector duct is larger than the nozzle exit, there is an additional expansion from the nozzle exit to the diffuser duct. Even if a single-phase fluid leaves the nozzle, fluid condensation could start in the free-jet expansion before reaching the duct resulting in a higher cell pressure.

The thermal equilibrium saturation curve for both hydrogen and helium are never crossed by the isentropic expansion curve for the stagnation conditions investigated. Since hydrogen and helium pumped essentially the same $P_c/P_t = 0.000684$ (Fig. 9) in the same configuration (configuration 2) and since the fluids (hydrogen and helium) remained single phase throughout the expansion, then $\gamma$ and $A_d/A^*$ are apparently the only parameters on which $P_c/P_t$ depends. By having the same configuration for both hydrogen and helium; then the $A_d/A^*$ was the same for the two gases resulting in an effective equal $\gamma$ of 1.67.

The isentropic expansion curve for argon crossed the thermal equilibrium curve and extended far into the two-phase fluid region (Fig. 11). This two-phase fluid expansion resulted in a high degree of condensation even when a high supersaturated state had been reached. The high degree of condensation resulted in a lower Mach number and higher static pressure at the nozzle exit than would have been if no condensation existed in the argon expansion. This low Mach number and high static pressure at the nozzle exit in effect was the same as having a smaller area ratio nozzle which results in a higher cell pressure. This result is shown in Fig. 9. The $P_c/P_t$ was 0.00166 for argon and 0.000683 for helium in the same configuration. Since the $\gamma$'s for both gases were essentially equal ($\gamma = 1.67$), then the condensation effect produced the difference shown in $P_c/P_t$.

The nitrogen and air $P_c/P_t$ performance is essentially the same for corresponding configurations 1 and 2. This equal performance was expected since both gases had essentially the same $\gamma$ for the conditions investigated (Fig. 5), and the condensation effects for the two gases in the same configuration were practically equal (Fig. 10).

A rather large change in $\gamma$ with temperature is evident in Fig. 5 for gaseous hydrogen below 500°R. Only a small change in $\gamma$ with temperature is noticeable in Fig. 5 for gaseous air, nitrogen, argon, and helium below 500°R. If an invariant $\gamma$ with temperature and pressure single-phase (gaseous phase) gas expands through a convergent-divergent nozzle into a two-phase region as does air, nitrogen, and argon in this investigation, then the $\gamma$ will decrease with an increase in condensation concentration according to Ref. 25 (pp 40-44). From

Fig. 10, an increase in condensation from configuration 2 ($A_{ne}/A^* = 10.76$) to configuration 1 ($A_{ne}/A^* = 18.00$) is evident for the expansion into the two-phase region. The air, nitrogen, and argon driving fluids for the two configurations (1 and 2) have an apparent decrease in $\gamma$ effect resulting from an increase in $P_c/P_t$. The $P_c/P_t$ effect from the geometry differences is discussed in section 4.2. The influence on $P_c/P_t$ of the geometric difference and of the $\gamma$ decrease due to condensation is shown in Fig. 9.

## 5.0 SUMMARY OF RESULTS

The variation in diffuser-ejector performance with various driving fluids for this investigation may be summarized as follows:

1. Air, nitrogen, argon, and helium had essentially an invariant ratio of specific heats with pressure and temperature for a stagnation temperature below 600°R. The ratio of specific heats for hydrogen gas varied from 1.40 to 1.67 with temperature for a stagnation temperature below 600°R and is affected little by pressure.

2. The breakdown pressure ratio for hydrogen in percent of one-dimensional normal shock total pressure ratio ($P_{ty}/P_{tx}$) was 88.54 based on a $\gamma = 1.40$ which was approximately 2 percent lower than the breakdown pressure ratio for nitrogen. Since $\gamma$ for hydrogen varies with temperature below 600°R, the breakdown pressure ratio in percent of $P_{ty}/P_{tx}$ was based on a $\gamma = 1.40$ because the fluid static temperature rises through the stream shocks as the fluid approaches the diffuser exit. This results in a $\gamma$ decrease from 1.67 toward 1.40.

3. The optimum driving pressure of 300 psia resulted in the minimum cell-to-nozzle total pressure ratio, $P_c/P_t$, for air and nitrogen. This optimum pressure was used as the bases from which the desired driving pressure for argon, helium, and hydrogen were determined for equal nozzle throat Reynolds number per unit length.

4. The $P_c/P_t$ ratios for both air and nitrogen were approximately equal for the corresponding configurations. This was expected since air is 78 percent nitrogen, and both gases have essentially the same $\gamma = 1.40$ relationship with pressure and temperature. The vapor pressure saturation relationship for the two gases differs only by approximately 7°F.

5. The $P_c/P_t$ performance for argon varied greatly from that of helium even though argon and helium have essentially the same $\gamma$ relationship with temperature and pressure. The vapor pressure saturation relationship for argon and helium differ by as much as 120 to 160°F. The argon $P_c/P_t$ was higher than the helium $P_c/P_t$ by a factor of approximately 3 for configuration 2. The higher $P_c/P_t$ ratio obtained for argon was a result of the expansion to a two-phase fluid for argon, while the expansion of helium was a single-phase gaseous fluid.

6. Hydrogen gas (below 600°R) as a driving fluid in configuration 2 ($A_d/A^* = 20.40$) gave a $P_c/P_t = 0.000684$ which was approximately equal to the $P_c/P_t$ obtained for helium. The temperature of the hydrogen gas at the nozzle exit ($A_{ne}/A^* = 10.76$) from an isentropic expansion was such that the $\gamma$ approached a limit of 1.67, which was approximately the same as $\gamma$ for helium ($\gamma = 1.66$). Hydrogen remained as a single gaseous phase fluid throughout the expansion through the nozzle.

7. A single-phase gaseous fluid with invariant $\gamma$ with temperature and pressure, such as nitrogen or argon, experiences a $\gamma$ decrease with an increase in condensation concentration when the single-phase gaseous fluid expands into the condensation region and becomes a two-phase fluid.

## REFERENCES

1. Wang, C. J., Peterson, J. B., and Anderson, R. "Gas Flow Tables." GM-TR-154, March 1957.

2. Bauer, R. C. and German, R. C. "Some Reynolds Number Effects on the Performance of Ejectors without Inducted Flow." AEDC-TN-61-87, August 1961.

3. Salisbury, J. Kenneth. Kent's Mechanical Engineers' Handbook, Power Volume. John Wiley and Sons, Inc., New York.

4. Hilsenrath, Joseph, Beckett, Charles W., et al. Tables of Thermal Properties of Gases. NBS Circular 564, U. S. Department of Commerce, 1955.

5. Arthur D. Little, Inc. "Hydrogen Handbook." AFFTC TR-60-19, April 1960.

6. Shapiro, Ascher H. The Dynamics and Thermodynamics of Compressible Fluid Flow, Volume 1. The Ronald Press Company, New York.

7. German, R. C. and Bauer, R. C. "Effects of Diffuser Length on the Performance of Ejectors without Induced Flow." AEDC-TN-61-89, August 1961.

8. Hale, James W. "Investigation of Two-Nozzle Cluster Diffuser-Ejector with and without Ejected Mass." AEDC-TDR-63-130, (to be published).

9. Jorgensen, Leland H. and Baum, Gayle M. "Charts for Equilibrium Flow Properties of Air in Hypervelocity Nozzle." NASA TN D-1333, September 1962.

10. Obert, Edward F. Thermodynamics. McGraw-Hill Book Company, Ind., New York.

11. Kiefer, Paul J., Kinney, Gilbert Ford, and Stuart, Milton C. Principles of Engineering Thermodynamics, 2nd Edition. John Wiley and Sons, Inc., New York.

12. Keenan, Joseph H. Thermodynamics. John Wiley and Sons, Inc., New York.

13. Goglia, Gennaro L. and Van Wylen, Gordon J. "Experimental Determination of Limit of Supersaturation of Nitrogen Vapor Expanding in a Nozzle." Journal of Heat Transfer, Vol. 83, Series C, No. 1, pp. 27-32, February 1961.

14. Daum, Fred L. "Air Condensation in a Hypersonic Wind Tunnel." AIAA Journal, Vol. 1, No. 5, pp. 1043-1046, May 1963.

15. Arthur, P. D. and Nagamatsu, H. T. "Experimental Supersaturation of Gases in Hypersonic Wind Tunnels." Memorandum No. 10. California Institute of Technology, Contract No. DA-04-495-Ord-19, July 15, 1952.

16. Willmarth, W. W. and Nagamatsu, H. T. "The Condensation of Nitrogen in a Hypersonic Nozzle." Journal of Applied Physics, Vol. 23, No. 10, pp. 1089-1095, October 1952.

17. Arthur, P. D. and Nagamatsu, H. T. "Effects of Impurities on the Supersaturation of Nitrogen in a Hypersonic Nozzle." Memorandum No. 7. California Institute of Technology, Contract No. DA-04-495-Ord-19, March 1, 1952.

18. Nagamatsu, H. T. and Willmarth, W. W. "Condensation of Nitrogen in a Hypersonic Nozzle." Memorandum No. 6. California Institute of Technology, Contract No. DA-04-495-Ord-19, January 15, 1952.

19. Charyk, Joseph V. and Lees, Lester. "Condensation of the Components of Air in Supersonic Wind Tunnels." Princeton University Aeronautical Engineering Laboratory Report No. 127, March 1948.

20. Arthur, P. D. and Nagamatsu, H. T. "Effects of Impurities in the Supersaturation of Nitrogen in a Hypersonic Nozzle." Heat Transfer and Fluid Mechanics Institute, pp 125-137, 1952.

21. Grey, J. and Nagamatsu, H. T. "The Effects of Air Condensation of Properties of Flow and Their Measurement in Hypersonic Wind Tunnels." Memorandum No. 8. California Institute of Technology, Contract No. DA-04-495-Ord-19, June 15, 1952.

22. Stever, H. Guyford and Rathbun, Kennetch C. "Theoretical and Experimental Investigation of Condensation of Air in Hypersonic Wind Tunnels." NACA TN 2559, November 1951.

23. Becker, John V. "Results of Recent Hypersonic and Unsteady Flow Research at the Langley Aeronautical Laboratory." Journal of Applied Physics, Vol. 21, No. 7, pp. 619-628, July 1950.

24. Faro, T., Small, T. R., and Hill, F. K. "The Supersaturation of Nitrogen in a Hypersonic Wind Tunnel." Journal of Applied Physics, Vol. 23, No. 1, pp. 40-43, January 1952.

25. Dobbins, Thomas O. "Thermodynamics of Rocket Propulsion and Theoretical Evaluation of Some Prototype Propellant Combinations." WADC TR-59-757, December 1959.

## APPENDIX I

## EQUAL REYNOLDS NUMBER SIMULATION

To have dynamic similarity in test results with different fluids, Reynolds number continuity must be achieved. Reynolds number is defined as follows:

$$Re = \frac{\rho V \ell}{\mu} \tag{I-1}$$

where

$\rho$ = Fluid density, $lb_m/ft^3$

V = Fluid velocity, ft/sec

$\mu$ = Dynamic viscosity, $lb_m/ft\text{-}sec$

$\ell$ = Characteristic length, ft

Since from the definition of Mach number

$$V = M \sqrt{\gamma g_c RT} \tag{I-2}$$

and from the equation of state of a perfect gas

$$\rho = \frac{P}{RT} \tag{I-3}$$

then Eq. (I-1) becomes

$$\frac{Re}{\ell} = \frac{\frac{P}{RT} M \sqrt{\gamma g_c RT}}{\mu} \tag{I-4}$$

By rearrangement, Eq. (I-4) becomes

$$\frac{Re}{\ell} = \frac{P \left[ M \sqrt{\frac{\gamma g_c}{R}} \sqrt{\frac{T_t}{T}} \right] \frac{1}{\sqrt{T_t}}}{\mu} \tag{I-5}$$

But

$$\dot{m} = M \sqrt{\frac{\gamma g_c}{R}} \left[ 1 + \frac{\gamma - 1}{2} M^2 \right]^{1/2} \tag{I-6}$$

and

$$\frac{T_t}{T} = 1 + \frac{\gamma - 1}{2} M^2 \tag{I-7}$$

which gives for Eq. (I-6)

$$\dot{m} = M \sqrt{\frac{\gamma g_c}{R}} \sqrt{\frac{T_t}{T}} \tag{I-8}$$

When Eq. (I-8) is substituted in Eq. (I-5), the following equation results:

$$\frac{Re}{\ell} = \frac{P \dot{m}}{\mu \sqrt{T_t}} \tag{I-9}$$

Rearrangement of Eq. (I-9) gives

$$\frac{Re}{\ell} = \frac{\left(\frac{P}{P_t} \dot{m}\right) P_t}{\mu \sqrt{T_t}} \tag{I-10}$$

The mass flow Eq. is

$$\frac{W}{A^*} = \frac{\left(\frac{P}{P_t} \dot{m}\right) P_t}{\sqrt{T_t}} \tag{I-11}$$

When Eq. (I-11) is substituted in Eq. (I-10), the result is

$$\frac{Re}{\ell} = \frac{W}{A^*} \frac{1}{\mu} \tag{I-12}$$

For a particular fluid flowing through a choked nozzle, the nozzle throat Reynolds number per unit length becomes from Eq. (I-10)

$$\frac{Re}{\ell} = K P_t \tag{I-13}$$

where

$$K = \frac{\left(\frac{P}{P_t} \dot{m}\right)_{M=1}}{\sqrt{T_t}\ \mu^*} \tag{I-14}$$

where K is a constant as long as the total temperature remains constant and the nozzle remains choked for a particular gas. Then for equal nozzle throat Reynolds number per unit length for the gases used in this investigation, the following equation must be satisfied:

$$(K P_t)_{air} = (K P_t)_{N_2} = (K P_t)_A = (K P_t)_{H_2} = (K P_t)_{He} \tag{I-15}$$

The nozzle throat static temperature was chosen for the basis of determining the Reynolds number per unit length continuity for the various gases.

TABLE 1

GAS CONSTANTS

| DRIVING GAS | SPECIFIC GAS CONSTANT, $R$, $\frac{ft\text{-}lb_f}{lb_m\text{-}^oR}$ | AVERAGE RATIO OF SPECIFIC HEATS ABOVE 0°F, $\gamma$ | AVERAGE SPECIFIC HEAT AT CONSTANT PRESSURE ABOVE 0°F, $C_p$, $\frac{Btu}{lb_m\text{-}^oR}$ | DYNAMIC VISCOSITY AT 70°F, $\mu$, $\frac{lb_m}{ft\text{-}sec}$ | MACH FUNCTION BASED ON AVG. $\gamma$ ABOVE 0°F, $\left(\frac{p}{p_t}\dot{m}\right)_{M=1}$ |
|---|---|---|---|---|---|
| Air | 53.321 | 1.401 | 0.242 | $12.222 \times 10^{-6}$ | 0.5319 |
| Argon (A) | 38.679 | 1.667 | 0.124 | $15.184 \times 10^{-6}$ | 0.6624 |
| Helium (He) | 386.057 | 1.66 | 1.240 | $13.017 \times 10^{-6}$ | 0.2094 |
| Nitrogen ($N_2$) | 55.147 | 1.40 | 0.246 | $11.820 \times 10^{-6}$ | 0.5224 |
| Hydrogen ($H_2$) | 766.369 | 1.41 | 3.395 | $5.945 \times 10^{-6}$ | 0.1406<br>0.1486 for $\gamma = 1.66$ |

$$\left(\frac{p}{p_t}\dot{m}\right)_{M=1} = \sqrt{\frac{\gamma g_c}{R}\left(\frac{2}{\gamma+1}\right)^{\frac{\gamma+1}{\gamma-1}}}$$

## TABLE 2

## SUMMARY OF TEST DATA

| DRIVING FLJID | TEST AREA | TEST CONFIG. | GAS TEMP. IN PLENUM, $T_t$, °R | MACH NO., $M_d$ | REYNOLDS NO. INDEX, Re/ℓ | CELL-TO-DRIVING PRESSURE RATIO | | | STARTING AND OPERATING PRESSURE RATIO | | | DRIVING PRESSURE, $P_t$, psia |
|---|---|---|---|---|---|---|---|---|---|---|---|---|
| | | | | | | $(P_c/P_t)_{act}$ | $(P_c/P_t)_{isen}$ | $\frac{(P_c/P_t)_{act}}{(P_c/P_t)_{isen}}$ | $(P_{ex}/P_t)_{act}$ | $P_{ty}/P_{tx}$ | $\frac{(P_{ex}/P_t)_{act}}{P_{ty}/P_{tx}}$ | |
| Air | $T\text{-}5BR_1$ | 1 | 516 | 6.46 | 606,976 | 0.000474 | 0.000401 | 1.183 | 0.01683 | 0.02171 | 0.7752 | 309 |
| Argon | $T\text{-}5BR_1$ | 1 | 452 | 10.40 | 517,313 | 0.000720 | 0.000121 | 5.931 | 0.01426 | 0.01938 | 0.7358 | 228 |
| Nitrogen | $T\text{-}5BR_1$ | 1 | 460 | 6.46 | 568,446 | 0.000450 | 0.000401 | 1.123 | 0.01748 | 0.02171 | 0.8052 | 245 |
| Air | $T\text{-}5BR_1$ | 2 | 470 | 4.75 | 622,484 | 0.001084 | 0.002543 | 0.426 | 0.06095 | 0.07505 | 0.8121 | 281 |
| | | 2 | 470 | 4.75 | 446,879 | 0.001109 | 0.002543 | 0.436 | | 0.07505 | | 202 |
| | | 2 | 470 | 4.75 | 334,053 | 0.001205 | 0.002543 | 0.474 | | 0.07505 | | 151 |
| | | 2 | 470 | 4.75 | 225,691 | 0.001343 | 0.002543 | 0.528 | | 0.07505 | | 102 |
| | | 2 | 465 | 4.75 | 161,384 | 0.001444 | 0.002543 | 0.568 | | 0.07505 | | 72 |
| | | 2 | 465 | 4.75 | 114,352 | 0.001549 | 0.002543 | 0.609 | | 0.07505 | | 51 |
| Argon | $T\text{-}5BR_1$ | 2 | 450 | 6.61 | 663,959 | 0.001667 | 0.001056 | 1.579 | | 0.06832 | | 282 |
| | | 2 | 460 | 6.61 | 614,955 | 0.001668 | 0.001056 | 1.580 | | 0.06832 | | 268 |
| | | 2 | 460 | 6.61 | 584,801 | 0.001714 | 0.001056 | 1.623 | | 0.06832 | | 255 |
| | | 2 | 478 | 6.61 | 466,949 | 0.001619 | 0.001056 | 1.533 | | 0.06832 | | 215 |
| | | 2 | 465 | 6.61 | 470,931 | 0.001586 | 0.001056 | 1.502 | 0.06439 | 0.06832 | 0.9425 | 210 |
| Helium | $T\text{-}5BR_1$ | 2 | 460 | 6.61 | 467,731 | 0.000683 | 0.001056 | 0.647 | | 0.06832 | | 575 |
| | | 2 | 464 | 6.61 | 178,362 | 0.000892 | 0.001056 | 0.845 | | 0.06832 | | 223 |
| | | 2 | 495 | 6.61 | 164,712 | 0.000944 | 0.001056 | 0.894 | | 0.06832 | | 215 |
| | | 2 | 464 | 6.61 | 167,997 | 0.000919 | 0.001056 | 0.870 | | 0.06832 | | 210 |
| | Remote | 2 | 510 | 6.61 | 654,365 | 0.000607 | 0.001056 | 0.575 | | 0.06832 | | 866 |
| | Area | 2 | 505 | 6.61 | 180,971 | | 0.001056 | | 0.05700 | 0.06832 | 0.8343 | 250 |
| Hydrogen | Remote | 2 | 500 | 6.61 | 712,182 | 0.000684 | *0.001056 | 0.648 | | *0.06832 | | 651 |
| | Area | 2 | 500 | 6.61 | 234,134 | | *0.001056 | | 0.06645 | *0.06832 | *0.9726 | 214 |
| | | | | | | | | | | **0.07505 | **0.8854 | |
| Nitrogen | $T\text{-}5BR_1$ | 2 | 500 | 4.75 | 469,524 | 0.001090 | 0.002543 | 0.429 | | 0.07505 | | 234 |
| | | 2 | 490 | 4.75 | 487,580 | 0.001043 | 0.002543 | 0.410 | | 0.07505 | | 230 |
| | | 2 | 495 | 4.75 | 443,503 | 0.001086 | 0.002543 | 0.427 | | 0.07505 | | 210 |
| Nitrogen | Remote | 2 | 493 | 4.75 | 1,370,432 | 0.001093 | 0.002543 | 0.430 | | 0.07505 | | 650 |
| | Area | 2 | 493 | 4.75 | 843,315 | 0.001045 | 0.002543 | 0.411 | | 0.07505 | | 400 |
| | | 2 | 491 | 4.75 | 619,392 | 0.001090 | 0.002543 | 0.429 | | 0.07505 | | 300 |
| | | 2 | 490 | 4.75 | 515,886 | 0.001151 | 0.002543 | 0.453 | | 0.07505 | | 239 |
| | | 2 | 489 | 4.75 | 452,175 | 0.001244 | 0.002543 | 0.489 | | 0.07505 | | 213 |
| | | 2 | 487 | 4.75 | 446,604 | 0.001262 | 0.002543 | 0.496 | 0.06771 | 0.07505 | 0.9022 | 210 |

*Obtained for a $\gamma$ of 1.67
**Obtained for a $\gamma$ of 1.40

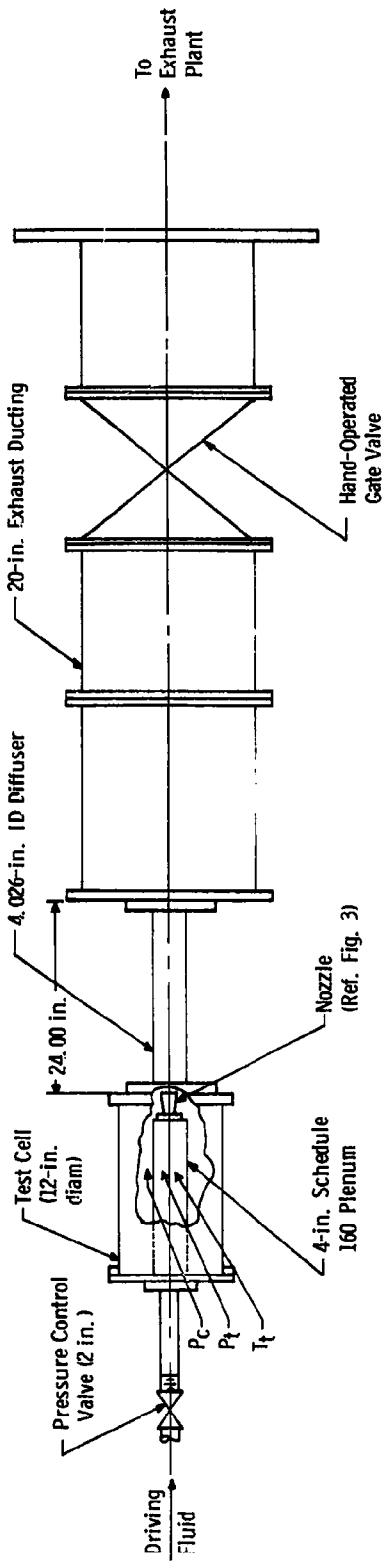


Fig. 1 Installation Schematic of Configuration 1

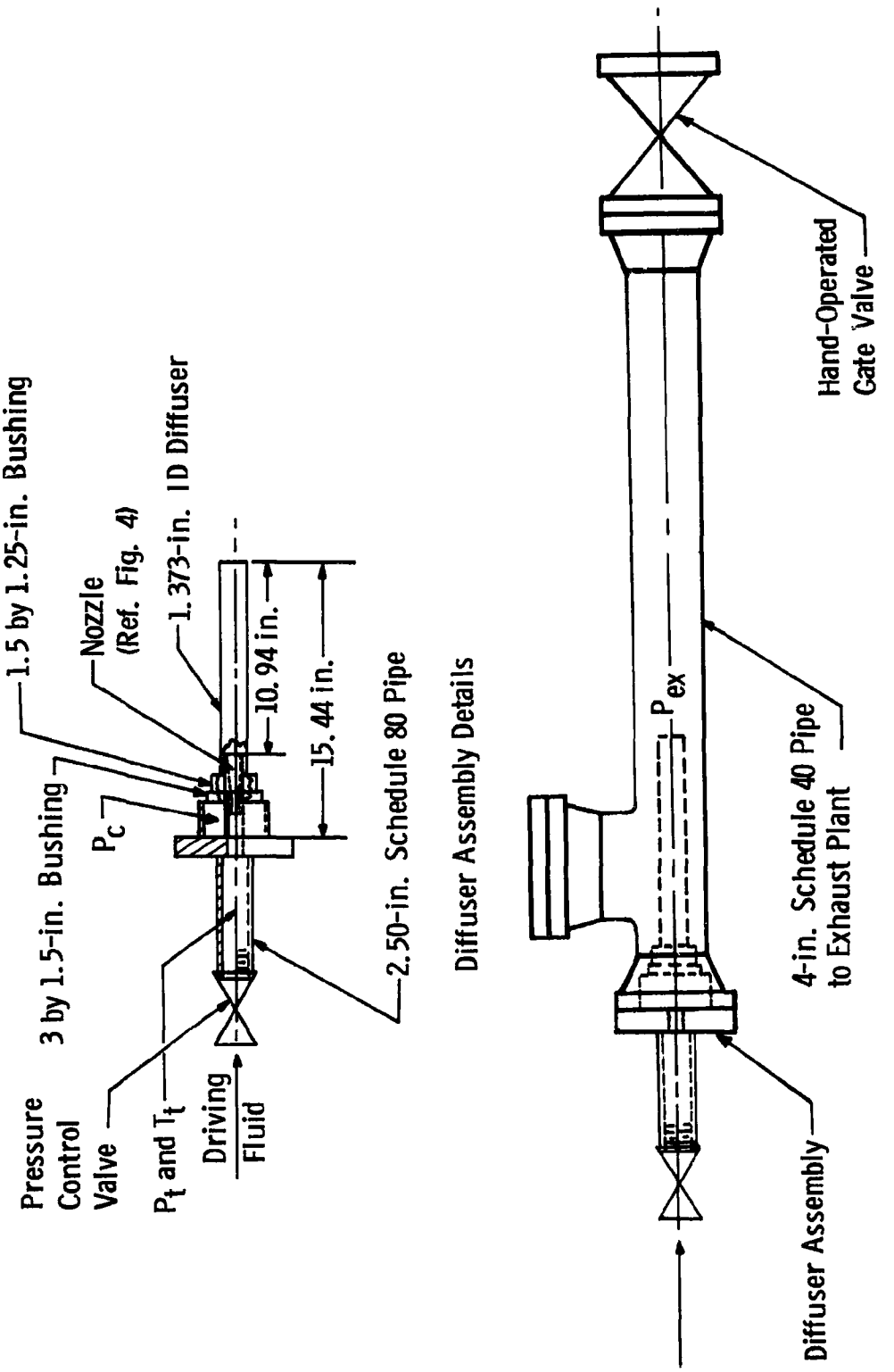


a. Diffuser Exhausting to RTF Exhaust Machines

Fig. 2 Installation Schematic of Configuration 2

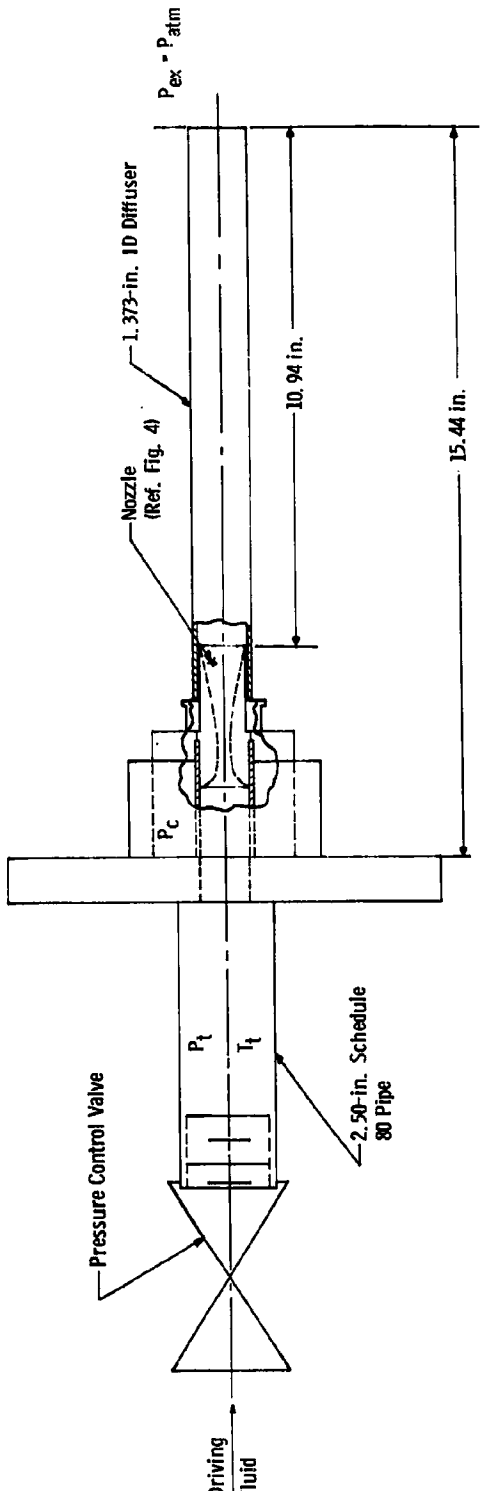


b. Diffuser Exhausting to Atmosphere in Remote Area

**Fig. 2 Concluded**

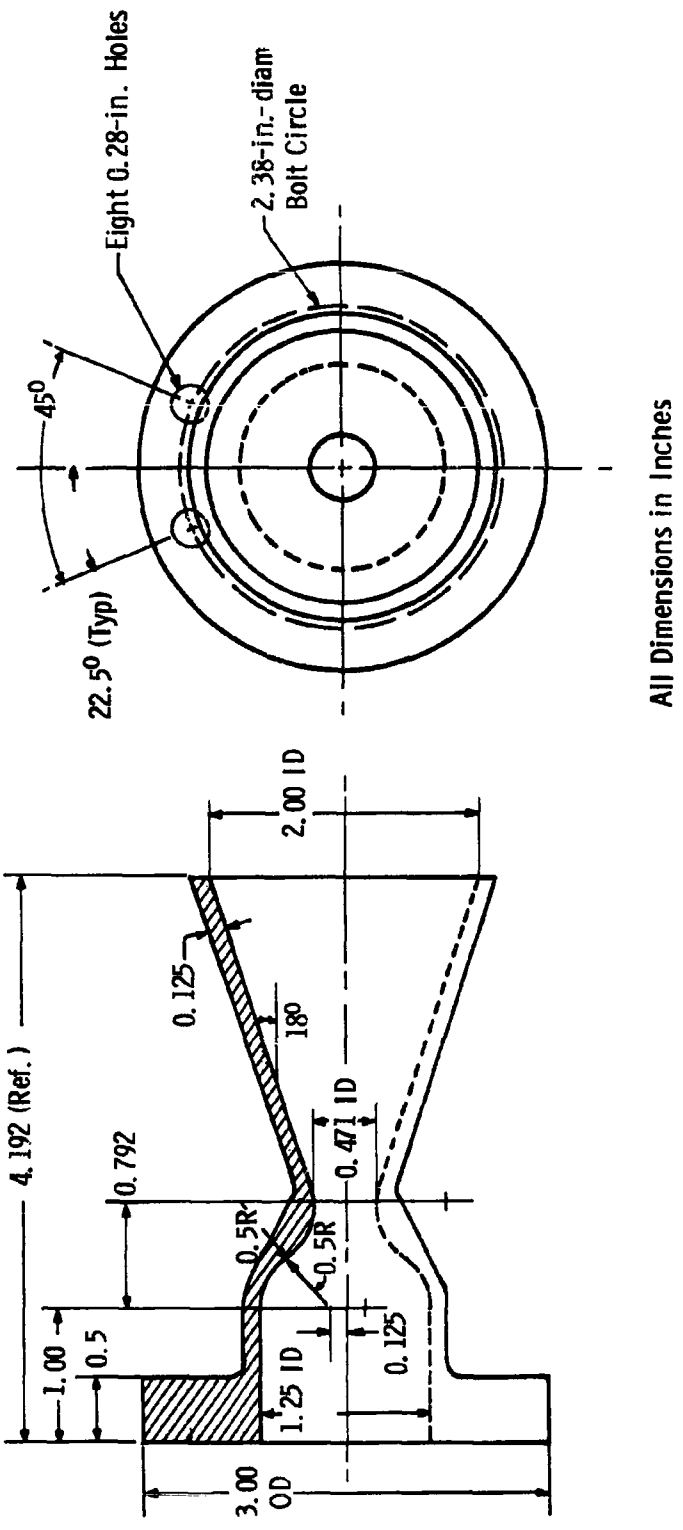


Fig. 3 Nozzle Details for Configuration 1

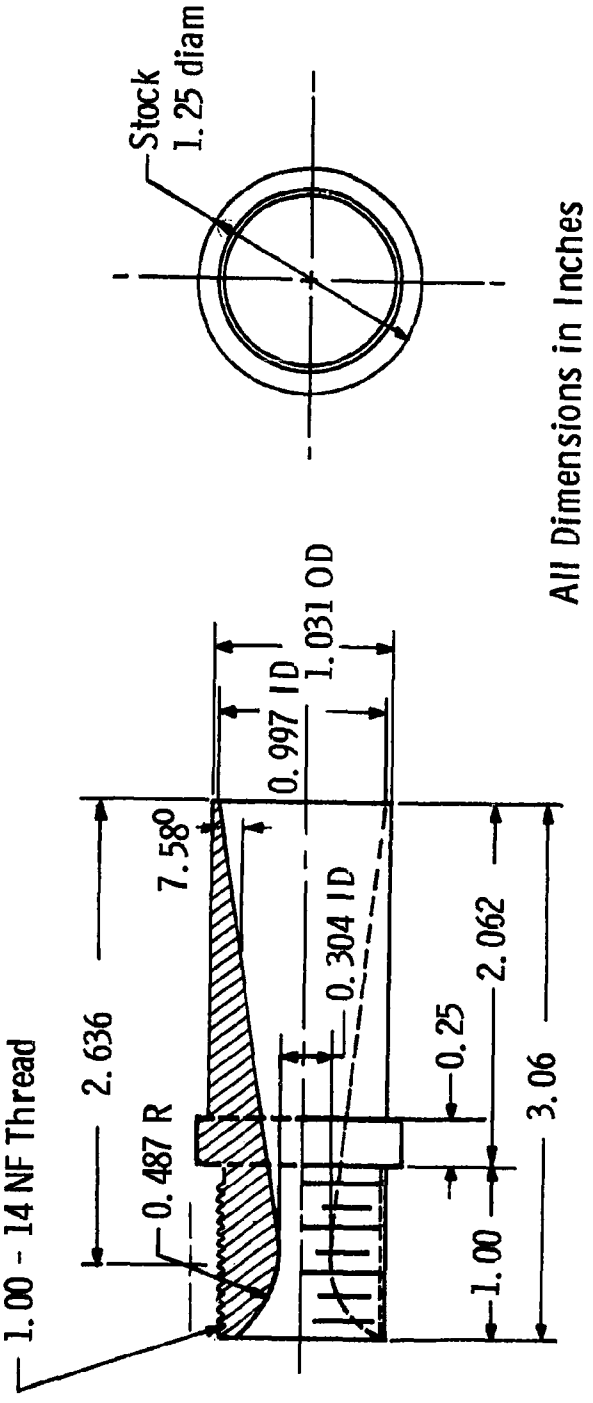


Fig. 4 Nozzle Details for Configuration 2

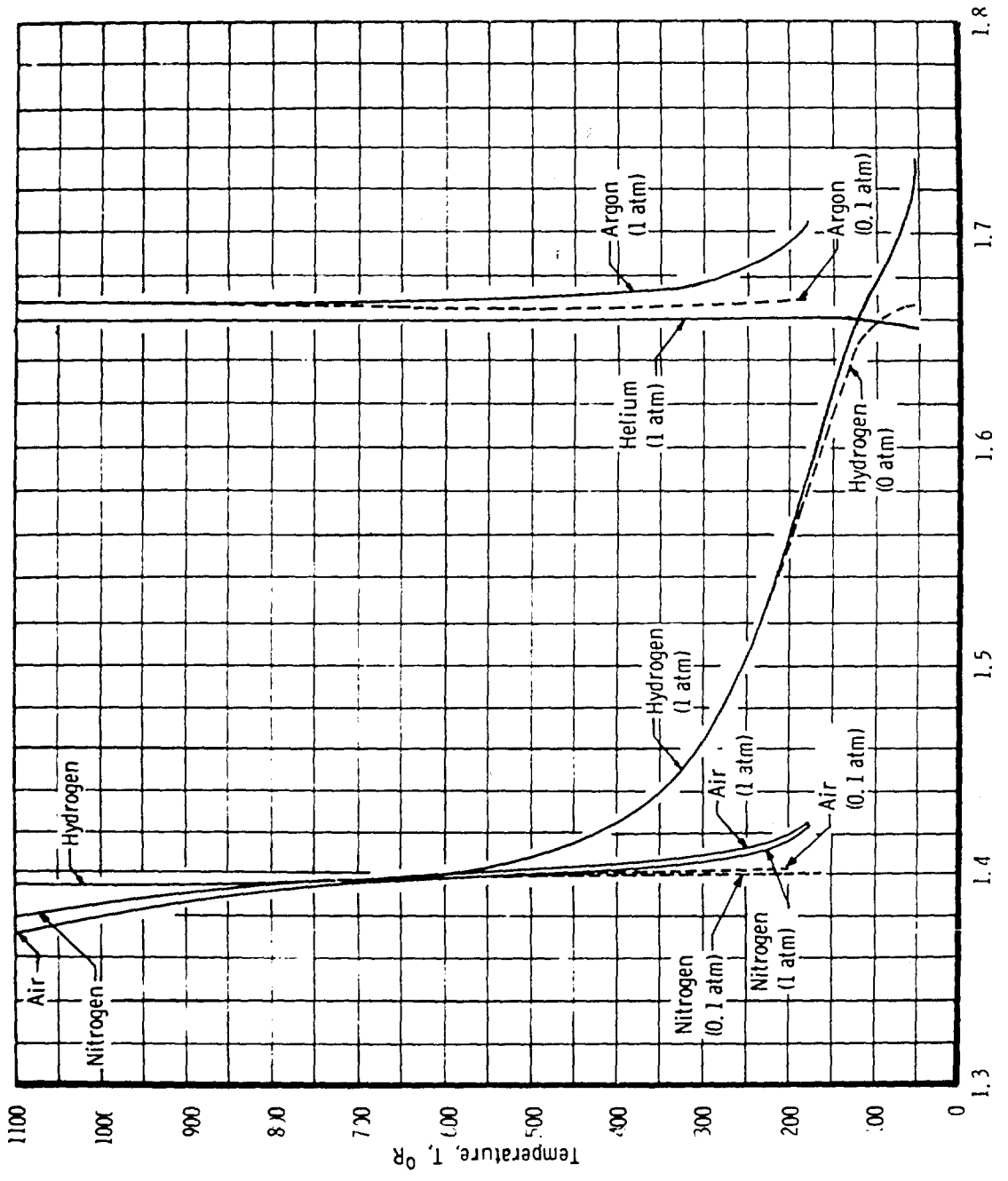


**Fig. 5 Variation of $\gamma$ with Temperature and Pressure**

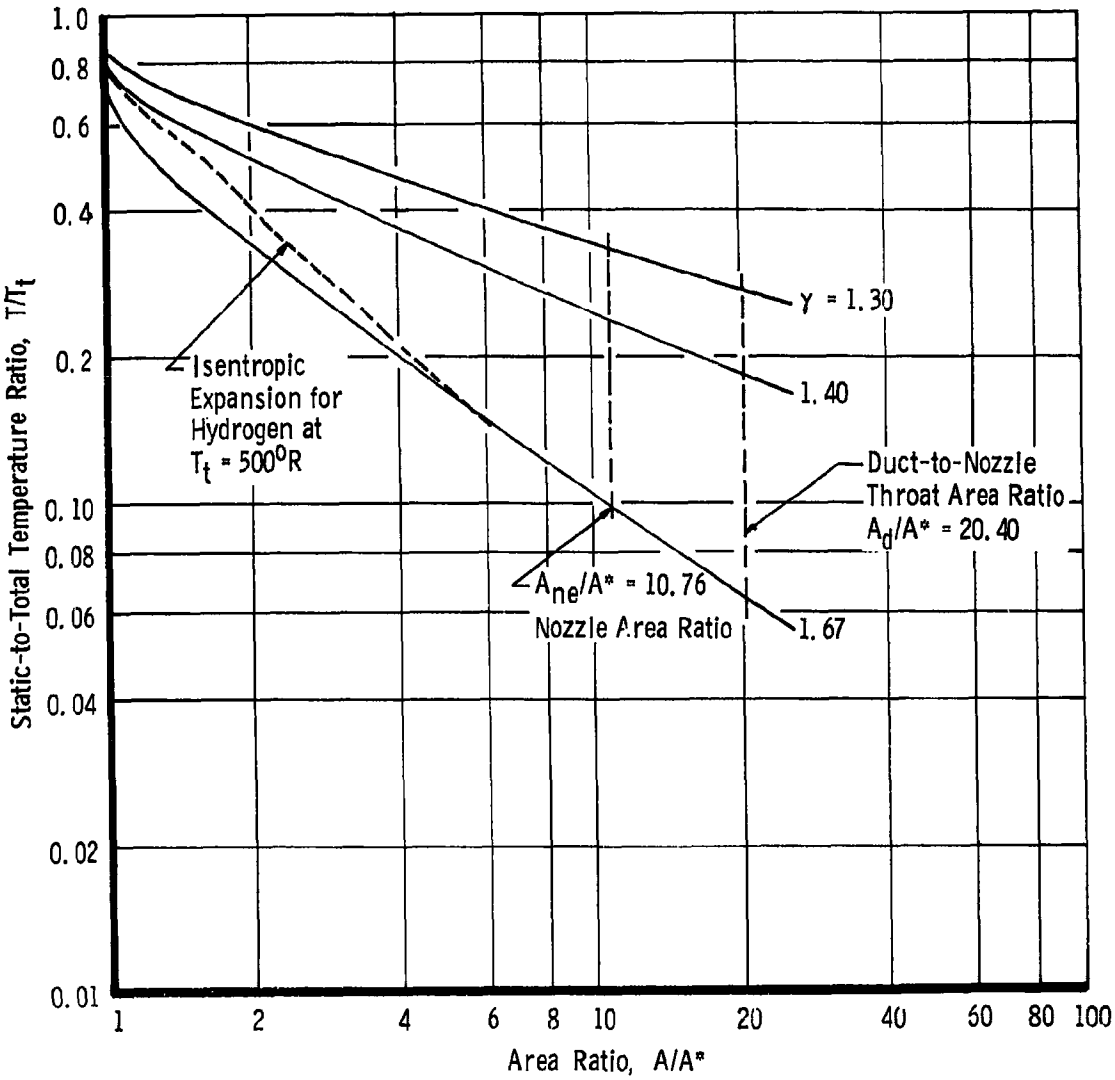


**Fig. 6 Static-to-Total Temperature Ratio Variation with Area Ratio for Isentropic Expansion for Different Constant $\gamma$'s and Variable $\gamma$**

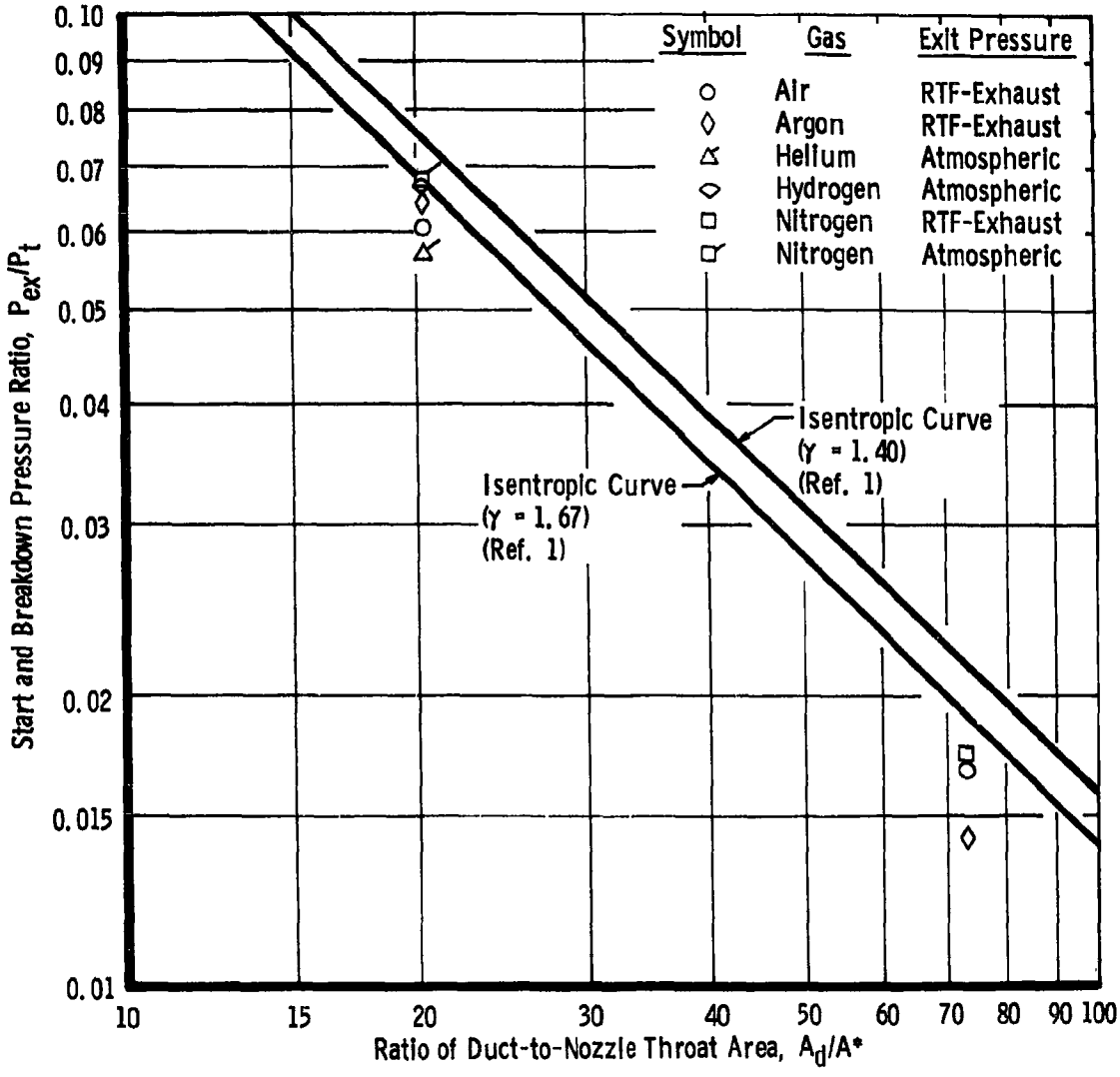


**Fig. 7 Diffuser-Ejector Average Pressure Ratio Required for Starting**

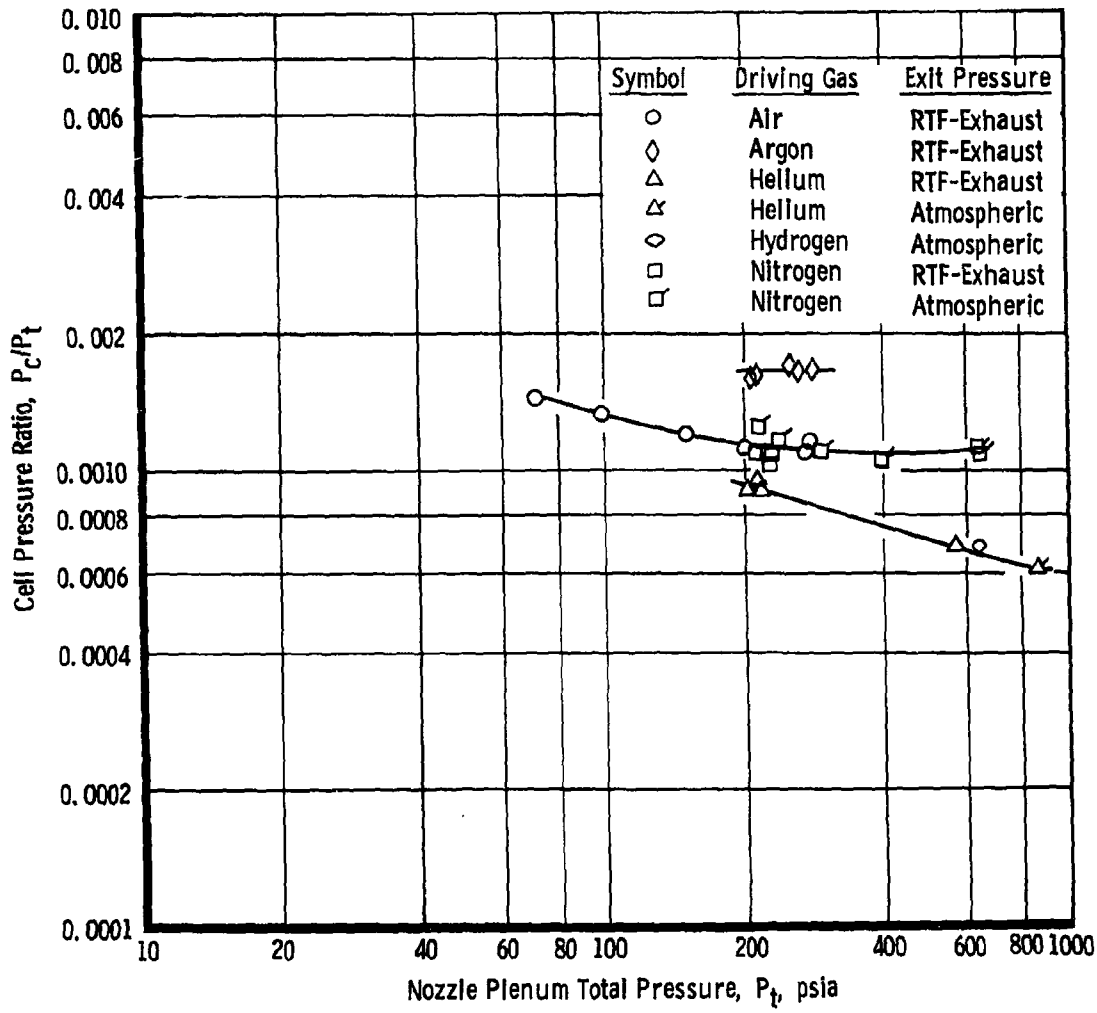


**Fig. 8 Variation of Minimum Cell Pressure Ratio, $P_c/P_t$, with Nozzle Plenum Total Pressure, $P_t$, for Configuration 2**

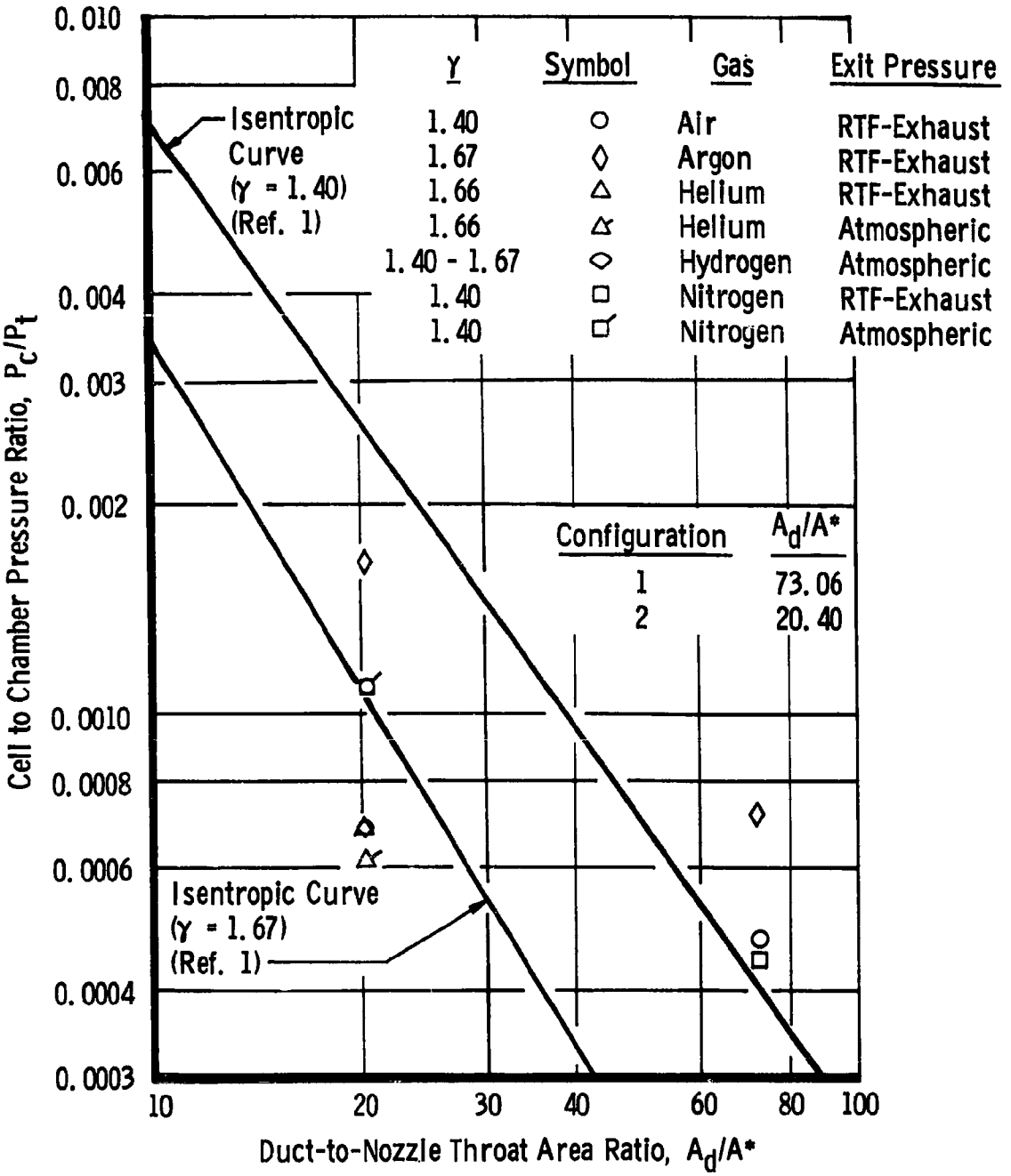


Fig. 9 Diffuser Cell-to-Driving Pressure Ratio Compared with One-Dimensional Isentropic Pressure Ratio

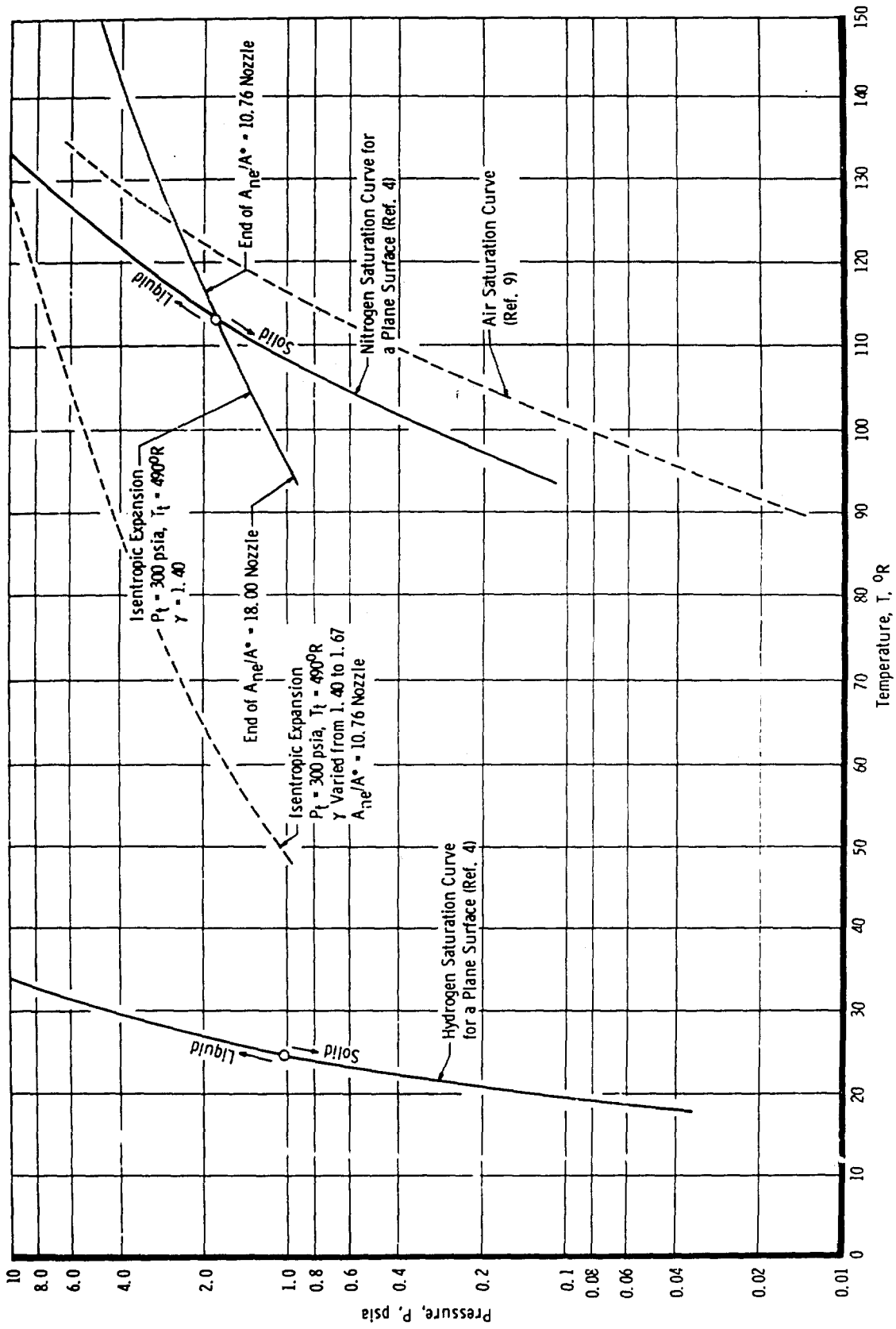


Fig. 10 Constant and Variable $\gamma$ Isentropic Expansion in Relation to Air, Nitrogen, and Hydrogen Saturation Curve

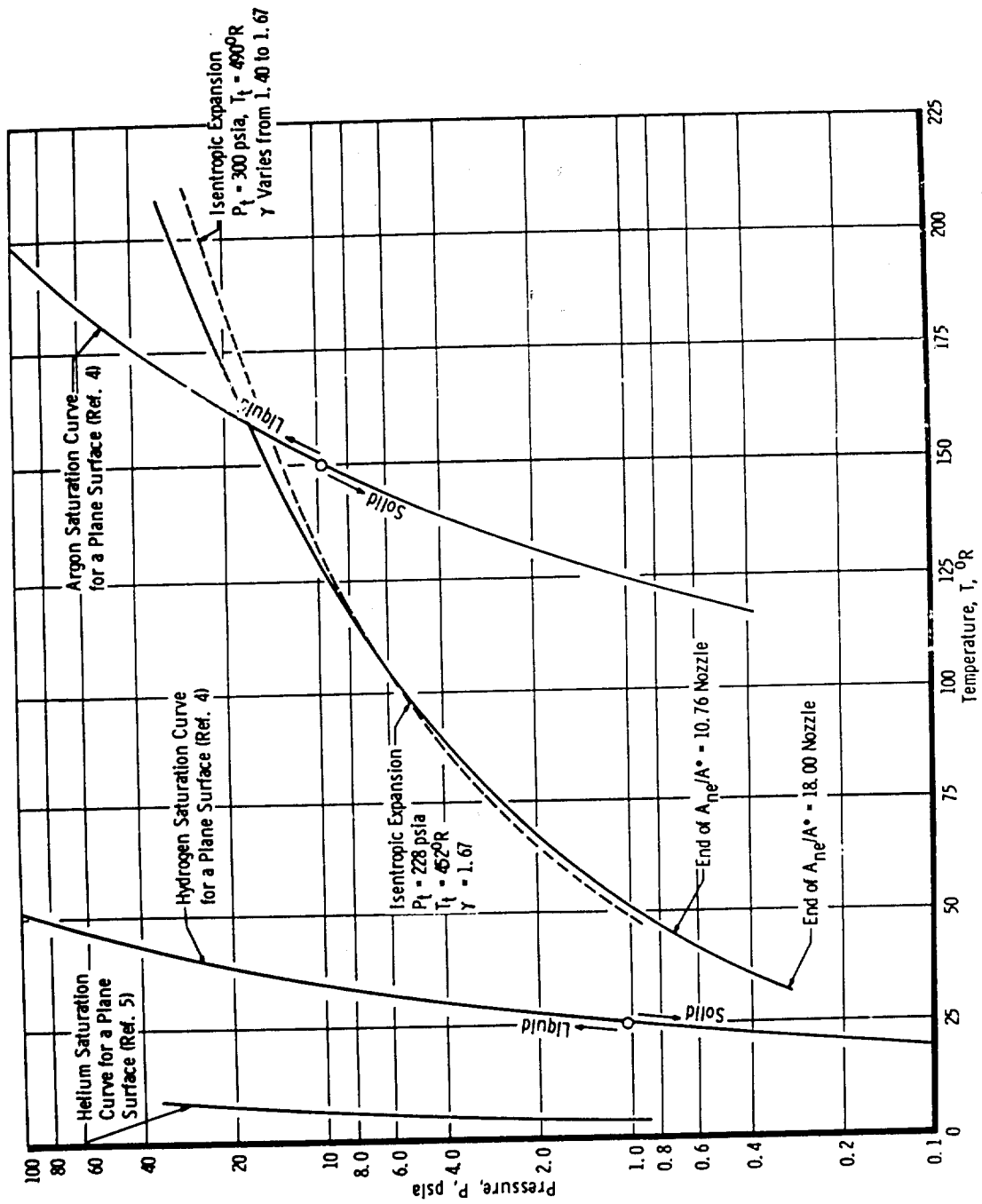


Fig. 11 Constant and Variable γ Isentropic Expansion in Relation to Argon, Hydrogen, and Helium Saturation Curve